Supporting Information

Local Symmetric Distortion Boosted Photon Up-conversion and Thermometric Sensitivity in Lanthanum Oxide Nanospheres

Hao Suo[a], Xiaoqi Zhao[a], Zhiyu Zhang[a], Rui Shi[b], Yanfang Wu[a], Jinmeng Xiang[a] and Chongfeng Guo[a*]

a. National Key Laboratory of Photoelectric Technology and Functional Materials (Culture Base) in Shaanxi Province, National Photoelectric Technology and Functional Materials & Application of Science and Technology International Cooperation Base, Institute of Photonics & Photon-Technology, Northwest University, Xi'an, 710069, China;

b. MOE Key Laboratory of Bioinorganic and Synthetic Chemistry, State Key Laboratory of Optoelectronic Materials and Technologies, School of Chemistry and Chemical Engineering, Sun Yat-sen University, Guangzhou 510275, China

---

Author to whom correspondence should be addressed

E-mail: guocf@nwu.edu.cn (Prof. Guo);

Tel & Fax: ±86-29-88302661

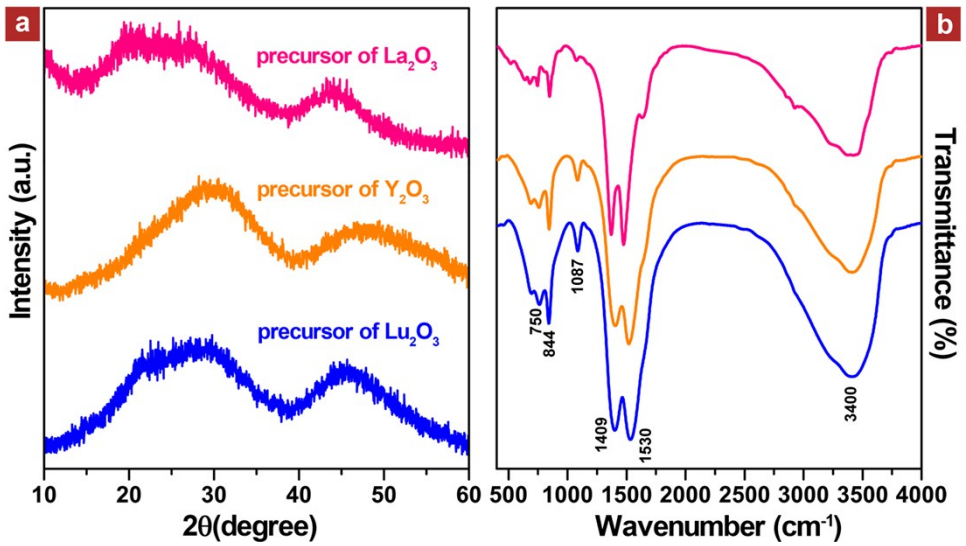

Figure S1. (a) XRD patterns and (b) FT-IR spectra of 2%Er^{3+}/3%Yb^{3+} co-doped three precursors. All precursor samples exhibited two broad bands without obvious diffraction peaks, which could be inferred as amorphous carbonate hydroxides $RE(OH)CO_3$ (RE = Lu, Y and La). Three precursor samples exhibited similar FT-IR spectra, in which the broad absorption band at around 3400 cm^{-1} were assigned to the stretching vibrations of hydroxyl groups. The absorption peaks centered at 750, 844 and 1087 cm^{-1} in the precursors were attributed to carbonate while the absorption at around 1409 and 1530 cm^{-1} corresponded to COO- group, which further confirmed the component of the precursors.

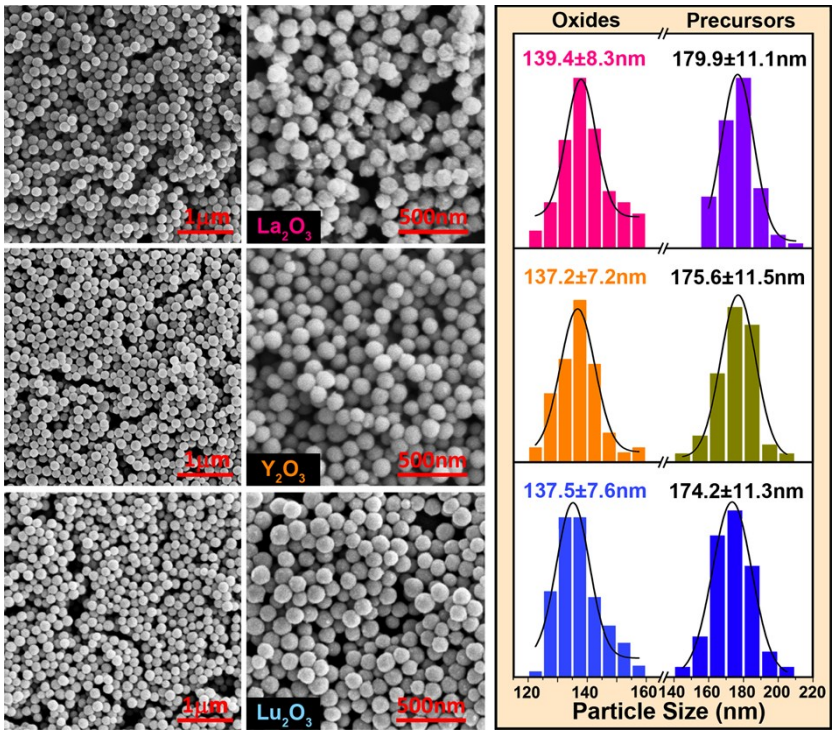

Figure S2. SEM images and size distributions of 2%Er^{3+}/3%Yb^{3+} co-doped precursor and final RE_2O_3 (RE = Lu, Y and La) samples. The precursor samples of Lu_2O_3, Y_2O_3 and La_2O_3 exhibited highly monodispersed and regular spherical shape with uniform size of about 174.2 ± 11.3, 175.6 ± 11.5 and 179.9 ± 11.1 nm, respectively. After heating treatment at 800 ^oC for 3 h, resulting RE_2O_3 particles still maintained highly dispersive and original spherical shape with rough surfaces and decreased size distributions of 137.2 ± 7.2, 137.5 ± 7.6 and 139.4 ± 8.3 nm.

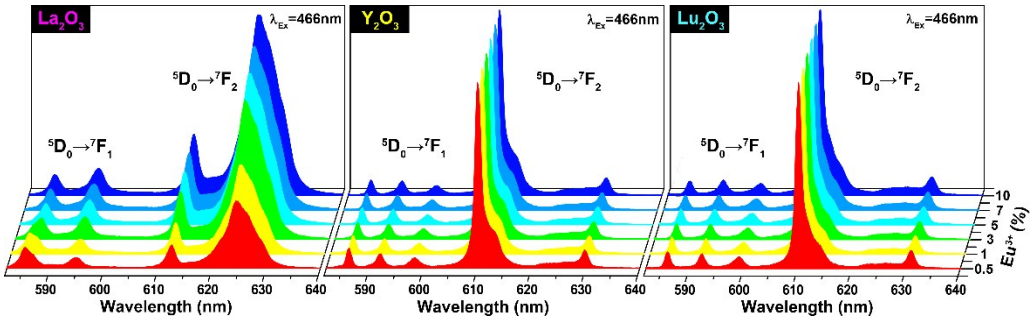

Figure S3. Emission spectra of RE_2O_3: xEu^{3+} (RE = Lu, Y and La; x = 0.5% ~ 10%) nanospheres ranging from 580 to 640 nm under 466 nm excitation. All the spectra were normalized at magnetic-dipole (MD) $^5D_0 \rightarrow {}^7F_1$ transition for better comparison. With increasing Eu^{3+} contents from 0.5% to 10%, the relative emission intensity from $^5D_0 \rightarrow {}^7F_2$ transition monotonously increased in La_2O_3 while maintained nearly unchanged in Lu_2O_3 and Y_2O_3 samples.

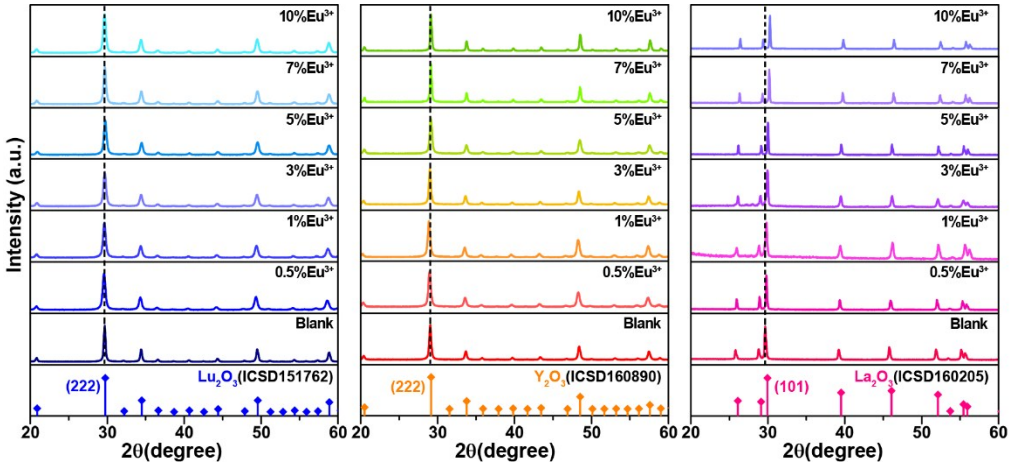

Figure S4. XRD patterns of RE_2O_3: xEu^{3+} (RE = Lu, Y and La; x = 0% ~ 10%) nanospheres along with their standard profiles. All the prepared samples are purity and well-crystallized without secondary phases.

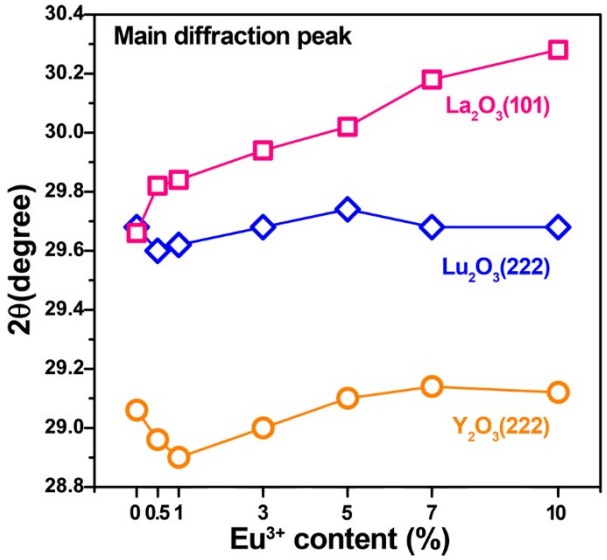

Figure S5. The shift of strongest diffraction peaks in XRD patterns of RE_2O_3: xEu^{3+} (RE = Lu, Y and La; x = 0% ~ 10%) nanospheres. Continuously shift of diffraction peaks (101) from low towards the higher angles was found with increasing Eu^{3+} contents in La_2O_3 due to the substitution of La^{3+} by Eu^{3+} ions with much smaller radius. However, no obvious shift was found in diffraction peaks (222) of Lu_2O_3 and Y_2O_3 samples as increasing Eu^{3+} contents. Above results indicated that the introduction of Eu^{3+} would result the lattice shrinkage of La_2O_3, yet barely affect the cell volumes of Lu_2O_3 and Y_2O_3 samples.

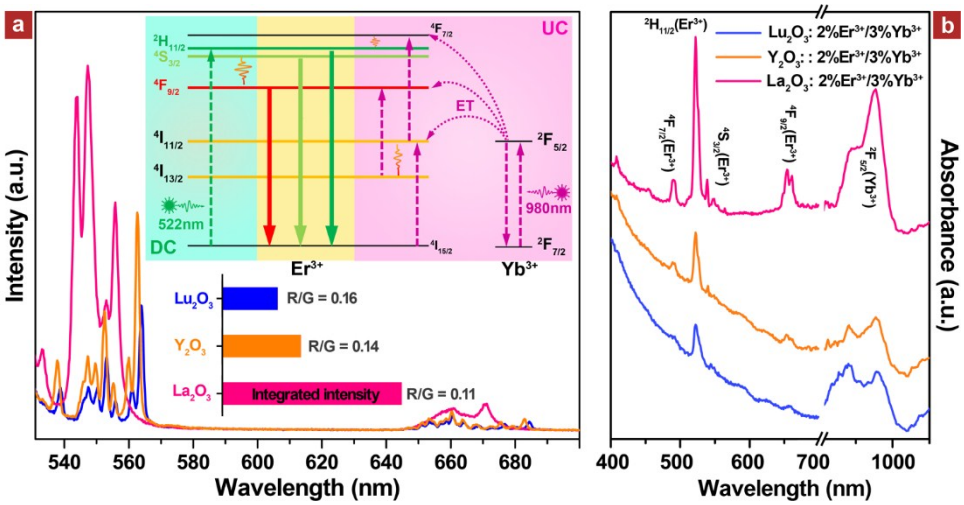

Figure S6. (a) DC emission spectra of RE_2O_3: 2%Er^{3+}/3%Yb^{3+} (RE = Lu, Y and La) nanospheres with corresponding integrated intensity and R/G ratio under 522 nm excitation, and the inset shows the simplified energy level diagram and possible energy transfer mechanisms in the DC and UC process; (b) UV-vis absorption spectra of three samples. Under 522 nm excitation, trigonal-phased La_2O_3 nanospheres exhibited about twice stronger visible emission than that of cubic-phased samples, and the DC emission intensity is mainly associated with the absorption ability around 522 nm and the radiative transition rates of emitting levels of Er^{3+}in three samples. This indicated that the lifetime of metastable states $^4I_{11/2}$ and $^4I_{13/2}$ plays a decisive role in determining UCL efficiency, as depicted in schematic energy level diagram. Local symmetric distortion enhanced f-f absorption and transition probabilities in La_2O_3 crystal could be further confirmed *via* UV-vis absorption spectra, from which the characteristic absorption bands at 490, 522, 539, 654 and 977 cm^{-1} corresponding to $^4F_{7/2}$, $^2H_{11/2}$, $^4S_{3/2}$, $^4F_{9/2} \rightarrow {}^4I_{15/2}$ of Er^{3+} and $^2F_{5/2} \rightarrow {}^2F_{7/2}$ of Yb^{3+} in La_2O_3 sample were all stronger than that in cubic samples.

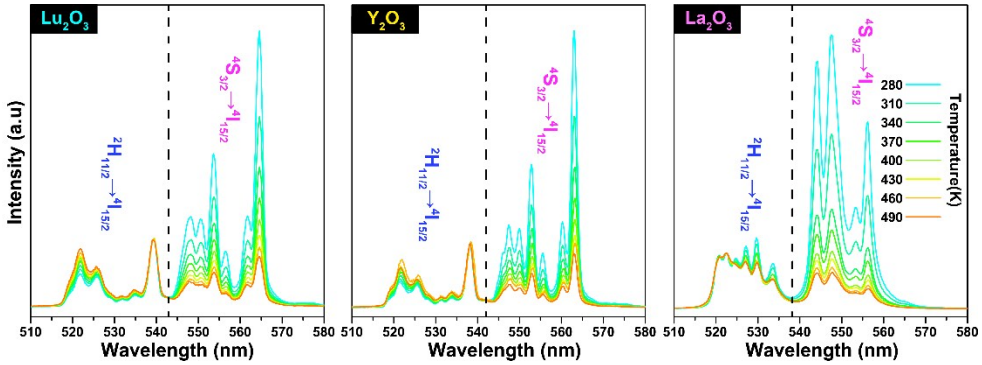

Figure S7. Temperature-dependent UC emission spectra of RE_2O_3: 2%Er^{3+}/3%Yb^{3+} (RE = Lu, Y and La) nanospheres within green region under 980 nm excitation (normalized at $^2H_{11/2} \rightarrow {}^4I_{15/2}$). With the increase of temperature from 280 to 490 K, the relative emission intensity of $^4S_{3/2} \rightarrow {}^4I_{15/2}$ monotonously declined in three samples without obvious change in band position.

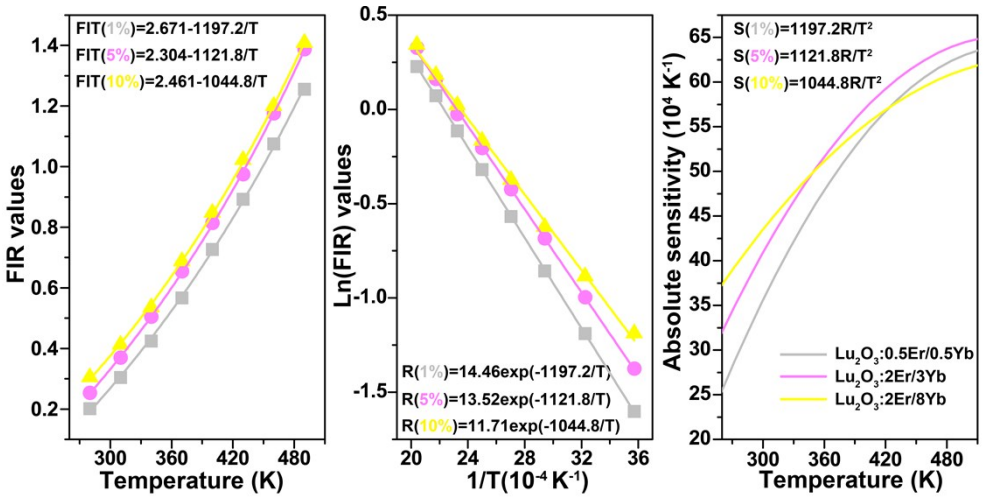

Figure S8. Temperature-dependent FIR and absolute sensitivity based on green emission in Lu_2O_3 doping with different Er^{3+}/Yb^{3+} contents under 980 nm excitation. According to the optimal fitting exponential curves of experimental points, the energy separation and coefficient B were found to be 825 cm^{-1} and 14.46 ($0.5\%Er^{3+}/0.5\%Yb^{3+}$), 775 cm^{-1} and 13.52 ($2\%Er^{3+}/3\%Yb^{3+}$), 721 cm^{-1} and 11.71 ($2\%Er^{3+}/8\%Yb^{3+}$), respectively. The obtained absolute sensitivity of samples gradually increased in our experimental range and reached to the maximum about 0.0063, 0.0064 and 0.0061 K^{-1} at the upper limit temperature 490 K.

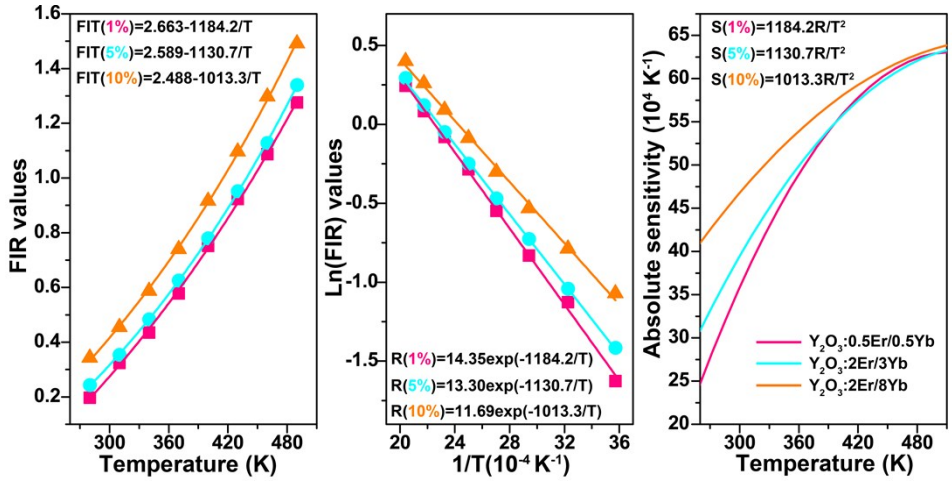

Figure S9. Temperature-dependent FIR and absolute sensitivity based on green emission in Y_2O_3 doping with different Er^{3+}/Yb^{3+} contents under 980 nm excitation. According to the optimal fitting exponential curves of experimental points, the energy separation and coefficient B were found to be 817 cm^{-1} and 14.35 ($0.5\%Er^{3+}/0.5\%Yb^{3+}$), 780 cm^{-1} and 13.3 ($2\%Er^{3+}/3\%Yb^{3+}$), 700 cm^{-1} and 11.69 ($2\%Er^{3+}/8\%Yb^{3+}$), respectively. The obtained absolute sensitivity of all samples gradually increased in our experimental range and reached to the maximum about 0.0063 K^{-1} at the upper limit temperature 490 K.

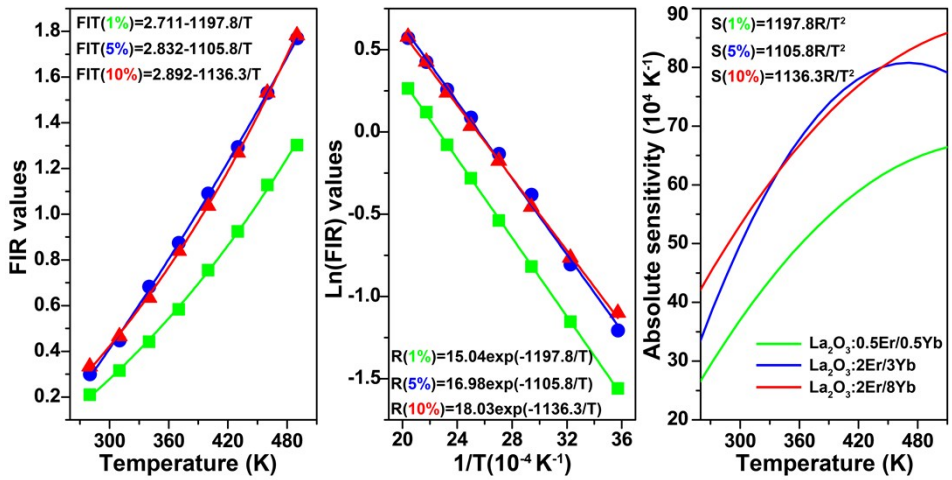

Figure S10. Temperature-dependent FIR and absolute sensitivity based on green emission in La_2O_3 doping with different Er^{3+}/Yb^{3+} contents under 980 nm excitation. According to the optimal fitting exponential curves of experimental points, the energy separation and coefficient B were found to be 825 cm^{-1} and 15.04 (0.5%Er^{3+}/0.5%Yb^{3+}), 763 cm^{-1} and 16.98 (2%Er^{3+}/3%Yb^{3+}), 784 cm^{-1} and 18.03 (2%Er^{3+}/8%Yb^{3+}), respectively. The obtained absolute sensitivity of three samples gradually increased in our experimental range and reached to the maximum about 0.0065, 0.0081 and 0.0085 K^{-1}at the upper limit temperature 490 K.

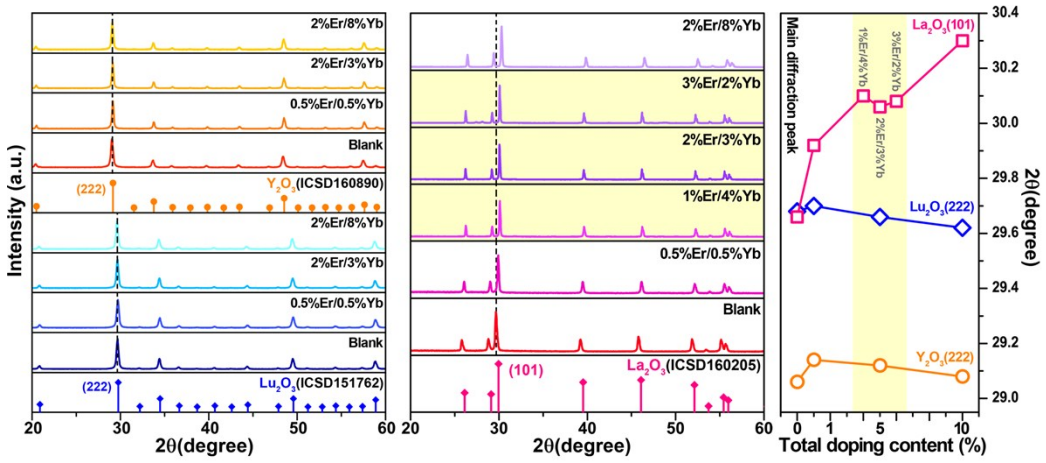

Figure S11. XRD patterns of RE_2O_3 (RE = Lu, Y and La) nanospheres doping with different Er^{3+}/Yb^{3+} contents and the corresponding shift of the strongest diffraction peaks. All the prepared samples are purity and well-crystallized without secondary phases. It is found that continuously shift of diffraction peaks (101) from low towards the higher angles was observed with increasing total contents of Er^{3+}/Yb^{3+} in La_2O_3 due to the substitution of La^{3+} by Er^{3+}/Yb^{3+} ions with much smaller radius, and the positions of (101) peak remained almost unchanged in La_2O_3 with 5% total doping content (1%Er^{3+}/4%Yb^{3+}, 2%Er^{3+}/3%Yb^{3+} and 3%Er^{3+}/2%Yb^{3+}). However, no obvious shift were observed in diffraction peaks (222) of Lu_2O_3 and Y_2O_3 samples as increasing Er^{3+}/Yb^{3+} contents. Above results indicated that the introduction of Er^{3+}/Yb^{3+} would result drastic lattice shrinkage of La_2O_3 crystal, yet barely affect the cell volumes of Lu_2O_3 and Y_2O_3 samples.

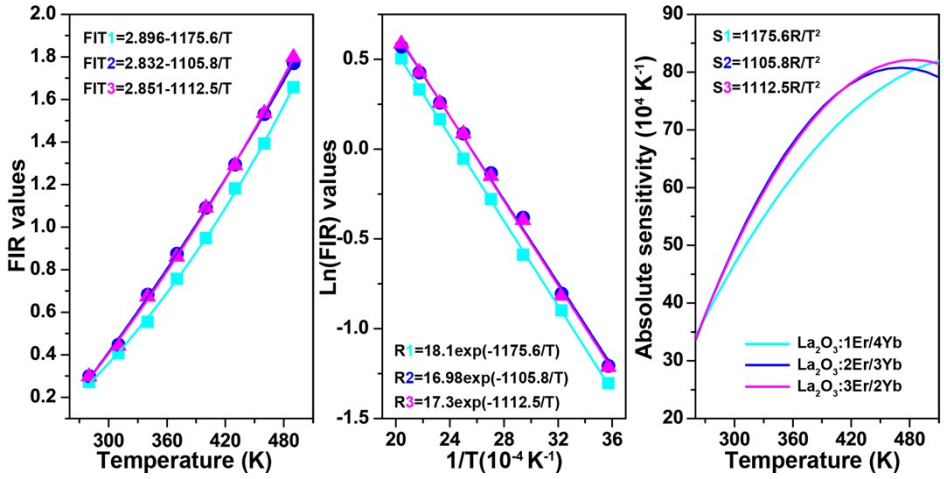

Figure S12. Temperature-dependent FIR and absolute sensitivity based on green emission in La_2O_3 samples doping with 5% total doping content under 980 nm excitation. According to the optimal fitting exponential curves of experimental points, the energy separation and coefficient B were found to be 810 cm^{-1} and 18.1 (1%Er^{3+}/4%Yb^{3+}), 763 cm^{-1} and 16.98 (2%Er^{3+}/3%Yb^{3+}), 767 cm^{-1} and 17.3 (3%Er^{3+}/2%Yb^{3+}), respectively. The obtained absolute sensitivity of three samples gradually increased in our experimental range and reached to the maximum about 0.0081, 0.0081 and 0.0083 K^{-1}at the upper limit temperature 490 K, indicating that the concentration-dependent energy transfer process hardly influence the sensitivity in present systems.

Table S1. Rietveld refinement and calculated crystallographic results for RE_2O_3: 2%Er^{3+}/3%Yb^{3+} (RE = Lu, Y and La) samples.

	Lu_2O_3: 2%Er^{3+}/3%Yb^{3+}	**Y_2O_3: 2%Er^{3+}/3%Yb^{3+}**	**La_2O_3: 2%Er^{3+}/3%Yb^{3+}**
Space group	*Ia-3*, cubic	*Ia-3*, cubic	*p-3m1*, trigonal
***a* (Å)**	10.3968	10.5971	3.9237
***b* (Å)**	10.3968	10.5971	3.9237
***c* (Å)**	10.3968	10.5971	6.1170
α, β, γ (deg)	90, 90, 90	90, 90, 90	90, 90, 120
***V* (Å^3)**	1123.83	1190.04	81.56
Z	16	16	1
R_{wp} (%)	4.806	4.778	4.473
R_p (%)	3.158	3.142	2.879

Table S2. The indexation of SAED patterns of RE_2O_3: 2%Er^{3+}/3%Yb^{3+} (RE = Lu, Y and La) nanospheres.

Samples	Crystal facets
Lu_2O_3: 2%Er^{3+}/3%Yb^{3+}	(211), (222), (321) and (400) of cubic-phased Lu_2O_3
Y_2O_3: 2%Er^{3+}/3%Yb^{3+}	(211), (222), (321) and (400) of cubic-phased Y_2O_3
La_2O_3: 2%Er^{3+}/3%Yb^{3+}	(100), (002), (102) and (110) of trigonal-phased La_2O_3

Table S3. Atomic distance of RE-RE in RE_2O_3: $2Er^{3+}/3Yb^{3+}$ (RE = Lu, Y and La) crystals.

Samples	RE-RE	Distance (Å)
Lu_2O_3: 2%Er^{3+}/3%Yb^{3+}	Lu2-Lu2	3.4563
Y_2O_3: 2%Er^{3+}/3%Yb^{3+}	Y2-Y2	3.5266
La_2O_3: 2%Er^{3+}/3%Yb^{3+}	La-La	3.7213

Table S4. The ionic radius of rare earth (RE^{3+}) ions with different coordination numbers

RE^{3+} ions	Ionic Radius (Å, CN = 6)	RE^{3+} ions	Ionic Radius (Å, CN = 7)
Lu^{3+}	0.86	La^{3+}	1.1
Y^{3+}	0.9		
Er^{3+}	0.89	Er^{3+}	0.94
Yb^{3+}	0.87	Yb^{3+}	0.92
Eu^{3+}	0.94	Eu^{3+}	1.01